J|A|C|S ARTICLES

Published on Web 04/01/2010

NMR Structural and Dynamical Investigation of the Isolated Voltage-Sensing Domain of the Potassium Channel KvAP: Implications for Voltage Gating

Zakhar O. Shenkarev,[†,*] Alexander S. Paramonov,[†] Ekaterina N. Lyukmanova,[†] Lyudmila N. Shingarova,[†] Sergei A. Yakimov,[†] Maxim A. Dubinnyi,[†] Vladimir V. Chupin,[†] Mikhail P. Kirpichnikov,[†] Marcel J. J. Blommers,[‡] and Alexander S. Arseniev*[,†]

Shemyakin-Ovchinnikov Institute of Bioorganic Chemistry, Russian Academy of Sciences, 16/10 Miklukho-Maklaya str., 117997 Moscow, Russia and Novartis Institutes for BioMedical Research, CH-4002 Basel, Switzerland

Received November 17, 2009; E-mail: zh@nmr.ru, aars@nmr.ru

Abstract: The structure and dynamics of the isolated voltage-sensing domain (VSD) of the archaeal potassium channel KvAP was studied by high-resolution NMR. The almost complete backbone resonance assignment and partial side-chain assignment of the $^{2}H,^{13}C,^{15}N$-labeled VSD were obtained for the protein domain solubilized in DPC/LDAO (2:1) mixed micelles. Secondary and tertiary structures of the VSD were characterized using secondary chemical shifts and NOE contacts. These data indicate that the spatial structure of the VSD solubilized in micelles corresponds to the structure of the domain in an open state of the channel. NOE contacts and secondary chemical shifts of amide protons indicate the presence of tightly bound water molecule as well as hydrogen bond formation involving an interhelical salt bridge (Asp62-R133) that stabilizes the overall structure of the domain. The backbone dynamics of the VSD was studied using ^{15}N relaxation measurements. The loop regions S1−S2 and S2−S3 were found mobile, while the S3−S4 loop (voltage-sensor paddle) was found stable at the ps−ns time scale. The moieties of S1, S2, S3, and S4 helices sharing interhelical contacts (at the level of the Asp62-R133 salt bridge) were observed in conformational exchange on the μs−ms time scale. Similar exchange-induced broadening of characteristic resonances was observed for the VSD solubilized in the membrane of lipid−protein nanodiscs composed of DMPC, DMPG, and POPC/DOPG lipids. Apparently, the observed interhelical motions represent an inherent property of the VSD of the KvAP channel and can play an important role in the voltage gating.

Introduction

The Na^{+}, K^{+}, and Ca^{2+} voltage-gated channels are a structurally related family of integral membrane proteins. Their conduction properties are modulated in response to changes in the transmembrane (TM) potential.[1,2] These channels are involved in a wide range of physiological phenomena, including the excitability of cardiac, muscle, and neuronal cells; propagation of nerve signals; and the secretion of hormones and neurotransmitters.[1,3,4] The spatial organization of voltage-gated channels is modular and involves a pore domain (PD) surrounded by a "ring" of four loosely associated voltage-sensing domains (VSDs) (Figure 1).[5,6] Due to their widespread abundance the VSDs represent important pharmacological targets for action of various neurotoxins[7,8] as well as for development of new drugs against various channelopathies.[2,3]

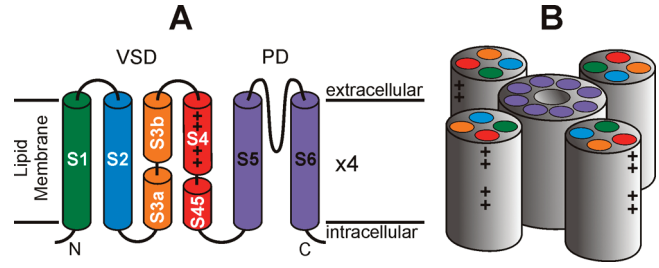

Figure 1. Schematic representations of the spatial organization of the KvAP channel in the cellular membrane. (A) One subunit from the full-length KvAP channel. The helices of the Voltage-Sensing Domain (VSD) (S1−S4) and of Pore Domain (PD) (S5, S6) are color coded. The positions of conservative Arg residues, responsible for voltage gating, are marked by crosses. (B) The tetrameric KvAP channel with one PD and four VSDs. Please note that the relative orientation of VSD to PD is not definitely known and can be different in different states (closed, open, inactivated open, etc.) of Kv channels.[12]

The VSD is composed of four consecutive TM helices (S1−S4). The S4 helix, sometimes called "voltage sensor", accommodates several positively charged residues (usually four

[†] Shemyakin-Ovchinnikov Institute of Bioorganic Chemistry.
[‡] Novartis Institutes for BioMedical Research.

(1) Hille, B. *Ion Channels of Excitable Membranes*, 3rd ed.; Sinauer Associates Inc.: Sunderland, MA, 2001.
(2) Ashcroft, F. M. *Ion channels and disease*; Academic Press: San Diego, CA, 2000.
(3) Borjesson, S. I.; Elinder, F. *Cell Biochem. Biophys.* **2008**, *52*, 149–174.
(4) Swartz, K. J. *Nature* **2008**, *456*, 891–897.
(5) Long, S. B.; Campbell, E. B.; MacKinnon, R. *Science* **2005**, *309*, 897–903.
(6) Long, S. B.; Tao, X.; Campbell, E. B.; MacKinnon, R. *Nature* **2007**, *450*, 376–382.

10.1021/ja909752r

Arg), which are directly involved in the channel gating.[3,4] It is generally assumed that the VSD experiences significant conformational rearrangement during voltage activation coupled with translocation of these positive charges from the intracellular to extracellular side of the membrane. This rearrangement induces conformational changes in the covalently linked PD (tetramer of S5−S6 helices) that leads to opening of the pore.[9] The majority of the available structural and biochemical data describes the VSD structure at zero TM potential that corresponds to the open or open inactivated state of the channel (activated state of VSD).[3,4] In contrast, the spatial structure of the VSD at resting TM potentials (approximately −100 mV) is presently unknown. Several descriptions for the mechanism of voltage gating have been proposed, but these suggestions are still under debate, and clearly new experimental data are needed.[6,10,11]

Solution state NMR allows the detailed characterization of the molecular dynamics of a membrane protein in a membrane mimicking environment.[13−16] The information about protein dynamics complements the structure provided by X-ray crystallography that provides a more static representation of the protein.[17] The study of structure and dynamics may result in more detailed models for protein function.[18,19] To better understand the functional dynamics of the voltage-sensing domains in K+ voltage-gated channels (Kv) we initiated an NMR investigation of the structure and dynamics of the isolated VSD of the KvAP channel. KvAP from the aerobic hyperthermophilic archaeon *Aeropyrum pernix* represents one of the well-studied voltage-gated potassium channels and can be considered as the prototype for Kv channels of higher animals.[20] The conformation of its VSD critically depends on its environment. For example, in the three published crystal structures (two structures of the full-length KvAP channel[21,22] and one of the isolated VSD[21]), the domain adopts significantly different spatial structures including the length of helical elements and their relative orientation. In contrast, the investigation of functional full-length KvAP and its isolated VSD in lipid bilayers by EPR spectroscopy shows that the domain structure is apparently the same,[12,23] indicating that the phospholipid membrane stands as a necessary supporting frame of the VSD structure. The EPR data were consistent only with the crystal structure of the isolated VSD, but not with other structures.[12,23]

The choice of an optimal detergent-based membrane mimetic for the here described NMR study was based on detergent screening (see our accompanying paper in this issue[24]). It was found that the VSD can adopt various conformations in detergents with different properties. The comparison of 2D ^{1}H,^{15}N-correlation spectra of the VSD/micelle preparations and VSD incorporated into lipid−protein nanodiscs (LPNs)[25−27] indicated that the conformation of the VSD in LPNs is maintained only in the environments based on zwitterionic detergents.[24]

The present report describes the results of an NMR study of the VSD in mixed DPC/LDAO micelles. The obtained resonance assignment and NOE connectivities were used to characterize the secondary and spatial structures of the domain in this medium. The comparison of these data with results of previous EPR and X-ray studies[21,23] indicates that the VSD in DPC/LDAO micelles adopts a similar structure as observed in the crystal state of the isolated domain as well as in the full-length active channel solubilized in liposomes at zero TM potential. The ^{15}N relaxation measurements revealed the defined patterns of "fast" ps−ns motions and "slow" μs−ms conformational fluctuations within the VSD backbone.

Results

Optimization of Experimental Conditions. The uniformly and selectively isotopically labeled VSD was obtained by expression in *E. coli* and extraction from membranes with DDM. The analysis of 2D ^{1}H,^{15}N-HSQC spectra of the VSD measured in DDM micelles (see our accompanying paper in this issue[24]) indicated that the conformation of the domain in this medium is similar to that in LPNs. The quality of the obtained NMR spectra, however, was insufficient for a detailed structural investigation.[24] Therefore, the protein was transferred to a detergent-based membrane mimetic that is better suited for structural studies. The results of detergent screening by NMR indicated that the environment of DPC micelles at neutral pH provides long-term stability to a "membrane-like" conformation of the VSD.[24] Unfortunately, complete backbone resonance assignment using the ^{2}H,^{13}C,^{15}N-labeled VSD was not possible at these experimental conditions because significant parts of S3 and S4 helices were not observable in NMR spectra (see Supporting Information). The quality of the VSD ^{1}H,^{15}N- HSQC spectra measured in DPC micelles at moderately acidic conditions (pH $\approx$ 5.0) was even worse. Moreover, the spectrum measured at low pH was different from the spectra of VSD incorporated in LPNs, indicating that the "membrane-like" conformation of the domain is only present at neutral pH (Figure S1).

(7) Alabi, A. A.; Bahamonde, M. I.; Jung, H. J.; Kim, J. I.; Swartz, K. J. *Nature* **2007**, *450*, 370–375.
(8) Bosmans, F.; Martin-Eauclaire, M. F.; Swartz, K. J. *Nature* **2008**, *456*, 202–208.
(9) Long, S. B.; Campbell, E. B.; MacKinnon, R. *Science* **2005**, *309*, 903–908.
(10) Broomand, A.; Elinder, F. *Neuron* **2008**, *59*, 770–777.
(11) Jiang, Y.; Ruta, V.; Chen, J.; Lee, A.; MacKinnon, R. *Nature* **2003**, *423*, 42–48.
(12) Chakrapani, S.; Cuello, L. G.; Cortes, D. M.; Perozo, E. *Structure* **2008**, *16*, 398–409.
(13) Sanders, C. R.; Sonnichsen, F. *Magn. Reson. Chem.* **2006**, *44*, S24–S40.
(14) Zhou, Y.; Cierpicki, T.; Jimenez, R. H.; Lukasik, S. M.; Ellena, J. F.; Cafiso, D. S.; Kadokura, H.; Beckwith, J.; Bushweller, J. H. *Mol. Cell* **2008**, *31*, 896–908.
(15) Hwang, P. M.; Kay, L. E. *Methods Enzymol.* **2005**, *394:335−50.*, 335–350.
(16) Tamm, L. K.; Abildgaard, F.; Arora, A.; Blad, H.; Bushweller, J. H. *FEBS Lett.* **2003**, *555*, 139–143.
(17) Wuthrich, K. *Angew. Chem., Int. Ed.* **2003**, *42*, 3340–3363.
(18) Ishima, R.; Torchia, D. A. *Nat. Struct. Biol.* **2000**, *7*, 740–743.
(19) Mittermaier, A. K.; Kay, L. E. *Trends Biochem. Sci.* **2009**, *34*, 601–611.
(20) Ruta, V.; Jiang, Y.; Lee, A.; Chen, J.; MacKinnon, R. *Nature* **2003**, *422*, 180–185.
(21) Jiang, Y.; Lee, A.; Chen, J.; Ruta, V.; Cadene, M.; Chait, B. T.; MacKinnon, R. *Nature* **2003**, *423*, 33–41.
(22) Lee, S. Y.; Lee, A.; Chen, J.; MacKinnon, R. *Proc. Natl. Acad. Sci U.S.A.* **2005**, *102*, 15441–15446.
(23) Cuello, L. G.; Cortes, D. M.; Perozo, E. *Science* **2004**, *306*, 491–495.
(24) Shenkarev, Z. O.; Lyukmanova, E. N.; Paramonov, A. S.; Shingarova, L. N.; Chupin, V. V.; Kirpichnikov, M. P.; Blommers, M. J. J.; Arseniev, A. S. *J. Am. Chem. Soc.* **2010** (DOI: 10.1021/ja9097498).
(25) Nath, A.; Atkins, W. M.; Sligar, S. G. *Biochemistry* **2007**, *46*, 2059–2069.
(26) Lyukmanova, E. N.; Shenkarev, Z. O.; Paramonov, A. S.; Sobol, A. G.; Ovchinnikova, T. V.; Chupin, V. V.; Kirpichnikov, M. P.; Blommers, M. J.; Arseniev, A. S. *J. Am. Chem. Soc.* **2008**, *130*, 2140–2141.
(27) Shenkarev, Z. O.; Lyukmanova, E. N.; Solozhenkin, O. I.; Gagnidze, I. E.; Nekrasova, O. V.; Chupin, V. V.; Tagaev, A. A.; Yakimenko, Z. A.; Ovchinnikova, T. V.; Kirpichnikov, M. P.; Arseniev, A. S. *Biochemistry (Mosc.)* **2009**, *74*, 756–765.

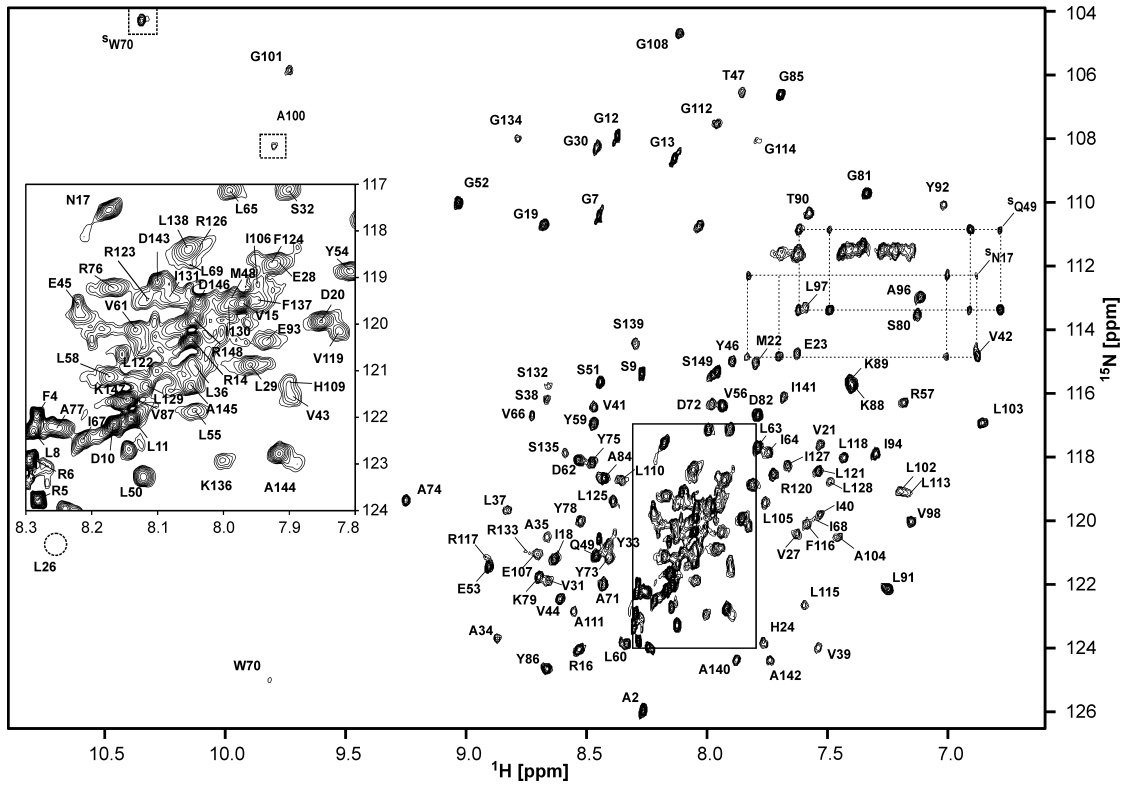

Figure 2. 2D ^{1}H,^{15}N-TROSY spectrum of VSD in DPC/LDAO mixed micelles. The spectrum was measured at 700 MHz for a 1 mM sample of ^{2}H,^{15}N-labeled VSD in a 100 mM perdeuterated d_{38}-DPC, 50 mM LDAO, pH 4.7, 42 °C. The obtained resonance assignments are shown. The resonances of side-chain groups are marked with superscript "s". The resonances of Asn and Gln NH_2 groups, observed as undecoupled multiplets in the sensitivity enhanced version of TROSY,[28] are connected by dotted lines. The boxed cross-peaks are folded in the ^{15}N dimension. The HN cross-peak of Leu26 (circled) is under the drawing threshold. The HN^{ϵ} resonances of Arg side chains are unassigned.

The results of NMR screening also point to the other detergent-based medium (weakly cationic LDAO micelles) that provides an environment for the "membrane-like" conformation of the VSD.[24] The ^{1}H,^{15}N-HSQC spectra of the VSD measured in LDAO micelles at moderately acidic pH demonstrated a lesser degree of exchange-induced signal broadening and consequently a larger number of observed cross-peaks than spectra of the protein obtained in DPC at neutral pH (Figure S1). Unfortunately, the VSD in pure LDAO micelles was unstable and underwent irreversible aggregation in a period of 1 week.[24] In an attempt to combine favorable properties of both detergents the VSD/DPC/LDAO samples were prepared with different DPC to LDAO molar ratios (from 9:1 to 1:9). The best quality ^{1}H,^{15}N-correlation spectra of the domain were obtained at pH $\approx$ 5.0 for the DPC/LDAO ratio 2:1. In addition this VSD/DPC/LDAO sample showed excellent stability during at least a half year of storage at room temperature (as judged by SDS-PAGE and ^{1}H,^{15}N-HSQC spectra).

NMR Resonance Assignment and Secondary Structure of Micelle-Solubilized VSD. The ^{1}H,^{15}N-TROSY spectrum of the ^{2}H,^{15}N-labeled VSD measured in DPC/LDAO (2:1) mixed micelles at pH 4.7 is shown in Figure 2. The large dispersion of $^{1}H^{N}$ backbone signals (from 6.8 to 10.7 ppm) indicates the presence of a well-defined tertiary structure of the domain. Broadening observed for a number of resonances points to the presence of μs−ms conformational fluctuations within the VSD molecule. The almost complete backbone resonance assignment (>90%) and partial side-chain assignment ($\sim$75% of $^{13}C^{\beta}$) were obtained for the VSD at these experimental conditions. The chemical shifts and sequential connectivities were extracted from TROSY versions of HNCA, HNCOCA, HNCACO, HNCO, and HNCACB spectra measured using the ^{2}H,^{13}C,^{15}N-labeled protein and from the CBCA(CO)HN spectrum acquired using the ^{13}C,^{15}N-labeled protein. In several "difficult" cases involving resonances broadened by conformational exchange the obtained assignment was based on the (i,i+1), (i,i+2), and (i,i+3) NOE connectivities observed in 3D ^{15}N-separated HNH-NOESY and ^{13}C,^{15}N-separated CNH-NOESY (τ_m 150 ms) spectra measured using ^{2}H,^{15}N- and ^{13}C,^{15}N-labeled samples, respectively. The selectively ^{15}N-Leu-labeled sample of the VSD was also used to facilitate sequential assignment. The obtained resonance assignment is shown in Figure 2. The selective broadening of several resonances (e.g., Leu26, Trp70, Ala100, etc.) is clearly evident from this spectrum.

A summary of the NMR data obtained for VSD is shown schematically in Figure 3. The identification of the secondary structure elements was done using secondary chemical shifts ($\Delta\delta$) for the $^{13}C^{\alpha}$, $^{13}C^{\beta}$, and $^{13}C'$ nuclei[29] and characteristic $H^{N}-H^{N}$ NOE connectivities.[30] These data were supplemented with observed protection of amide protons from exchange with solvent (water) and small temperature coefficients of chemical shifts of amide proton signals ($\Delta\delta^{1}H^{N}/\Delta T$),[31] which indicates possible formation of intramolecular hydrogen bonds or shielding from the solvent in the interior of the protein/detergent complex. The position of five helices (S1, S2, S23, S3b, and S4) were obtained from consecutive residues with positive values of $\Delta\delta^{13}C^{\alpha}$ and $\Delta\delta^{13}C'$, negative $\Delta\delta^{13}C^{\beta}$ values, the

(28) Nietlispach, D. *J. Biomol. NMR.* **2005**, *31*, 161–166.
(29) Wishart, D. S.; Case, D. A. *Methods Enzymol.* **2001**, *338*, 3–34.
(30) Wuthrich, K. *NMR of Proteins and Nucleic Acids*; John Wiley and Sons: New York, 1986.
(31) Baxter, N. J.; Williamson, M. P. *J. Biomol. NMR* **1997**, *9*, 359–369.

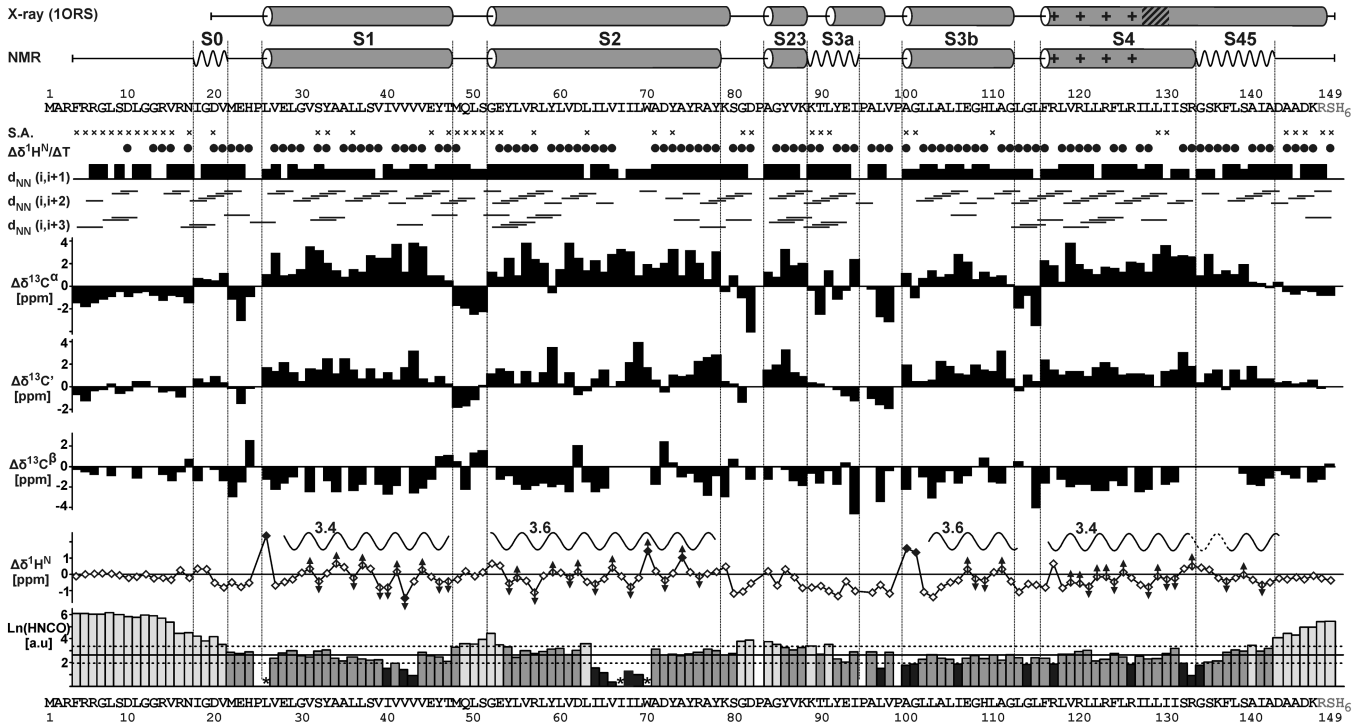

Figure 3. NMR data that define the secondary structure of the VSD. All measurements were done at 700 MHz for 1 mM samples of the $^{2}H,^{15}N$- or $^{2}H,^{13}C,^{15}N$-labeled VSD in 100 mM perdeuterated d_{38}-DPC, 50 mM LDAO, pH 4.7, 42 °C. (First line) Solvent accessibility (S.A.) of $^{1}H^{N}$ (crosses). The S.A. is determined by the presence of a cross-peak between the ^{1}H frequency of water and $^{1}H,^{15}N$ frequencies of the amide group in the 3D ^{15}N-separated HNH-NOESY spectrum (τ_m 150 ms). The presence of the cross-peak indicates either fast exchange of $^{1}H^{N}$ with solvent or spatial closeness of $^{1}H^{N}$ to the tightly bound water molecule (e.g., Leu63, Gly101), to the other solvent-exchangeable proton (e.g., $^{1}H^{O}$ of Tyr), or to the residual $^{1}H^{\alpha}$ (the estimated degree of ^{2}H incorporation in the protein is ~85%). The absence of the cross-peak indicates protection of $^{1}H^{N}$ from the solvent exchange. (Second line) The filled circles denote amide protons with temperature coefficients ($\Delta\delta^{1}H^{N}/\Delta T$) less than 4.5 ppb/K. Temperature coefficients were measured in the range 25−50 °C using 3D HNCO spectra. (Third, fourth, and fifth lines) Sequential and medium-range NOEs observed in the HNH-NOESY (τ_m 150 ms). (Sixth, seventh, eighth, and ninth lines) Deviation of the $^{13}C^{\alpha}$, $^{13}C'$, $^{13}C^{\beta}$, and $^{1}H^{N}$ chemical shifts from random coil values. Down-field values (positive deviation) of the $^{13}C^{\alpha}$ and $^{13}C'$ resonances and upfield value of the $^{13}C^{\beta}$ resonance indicate a backbone helical conformation. The apparent periodicity of $\Delta\delta^{1}H^{N}$ is shown by wavy lines, and the periodicity (residues per period/turn) is indicated above. The loss of periodicity between the S4 and S45 helices is marked by a dotted line. For clarity, the residues within S1, S2, S3b, S4, and S45 helical elements which demonstrate upfield or downfield $\Delta\delta^{1}H^{N}$ values relative to neighboring residues are marked by arrows. (The N-terminal fragments of S1, S2, S3b, and S4 were excluded from the analysis as the corresponding $\Delta\delta^{1}H^{N}$ values probably contain a contribution from the helical dipole.) The $^{1}H^{N}$ discussed in the text are marked by filled diamonds. (Tenth line) Intensity (log values) of peaks in 3D HNCO spectrum. The level corresponding to the average intensity (calculated over S1−S45) is shown by a solid line. The levels corresponding to twice smaller or twice larger intensities are shown by broken lines. The HNCO intensities are classified accordingly as weak, medium, and strong (black, gray and white-gray bars, respectively). The stars denote vanishing HNCO peaks. The secondary structure elements as found in the crystal of the isolated VSD[21] and as determined by NMR (present work) are shown above the protein sequence. The helices are shown by cylinders, and the "pseudohelical" segments are shown by wavy lines (see text for details). The position of the hinge between S4 and S45 as determined by EPR[23] is hatched. The conservative Arg residues that are responsible for voltage gating are marked. The cloning artifact residues are shown in gray.

presence of (i,i+1), (i,i+2) and (i,i+3) NOE contacts, protection from exchange with solvent, and small temperature coefficients. In addition, three "pseudohelical" segments (S0, S3a, and S45), with either irregular $\Delta\delta^{13}C$ patterns or the absence of solvent exchange protection, were observed. A comparison of the obtained data with the crystal structure of the isolated VSD[21] (see Figure 3, upper line) reveals only some discrepancies. The majority of them are the observed distortions in segments S3a and S45 and the presence of an additional "pseudohelical" element S0. In this respect, it should be noted that the enhanced solvent accessibility of S23−S3a helices was recently observed in the cysteine scanning mutagenesis study of KvAP,[32] and the presence of a hinge between S4 and S45 (representing one continuous helix in the crystal structure) was revealed by EPR of the full-length channel incorporated into a lipid bilayer.[23] On the other hand, the short element S0 was not observed by X-ray crystallography due to the absence of electron density in the N-terminus of the VSD. This segment involves only four residues (Ile18-Val21) and most probably represents one turn of a helix or a short sequence of β-turns. Interestingly, the VSD of mammalian Kv1.2/2.1 chimaeric channel also contains a short (~10 a.a.) homologous helical segment (S0), located at the membrane−water interface.[6]

Curvature of Transmembrane Helices and Interhelical Contacts of the Micelle-Solubilized VSD. The secondary chemical shifts for amide protons ($\Delta\delta^{1}H^{N}$, Figure 3) were used for a more detailed characterization of the VSD structure. The inspection of $\Delta\delta^{1}H^{N}$ patterns in S1, S2, S3b, S4, and S45 helices revealed the presence of the characteristic periodicity (Figure 3). The most prominent upfield (downfield) shifts were observed for each third or fourth residue. The periodic patterns are usually regarded as indicators of helical curvature.[33,34] In this case, the shortening of hydrogen bonds at the concave side of the helix induces downfield $^{1}H^{N}$ shifts and the lengthening of hydrogen

(32) Neale, E. J.; Rong, H.; Cockcroft, C. J.; Sivaprasadarao, A. *J. Biol. Chem.* **2007**, *282*, 37597–37604.

(33) Kuntz, I. D.; Kosen, P. A.; Craig, E. C. *J. Am. Chem. Soc.* **1991**, *113*, 1406–1408.

(34) Zhou, N. E.; Zhu, B.; Sykes, B. D.; Hodges, R. S. *J. Am. Chem. Soc.* **1992**, 4320–4326.

bonds at the convex face induces upfield shifts.[34,35] Inspection of the crystal structure of VSD[21] revealed the curvatures in S1, S2, S3b, and S4 helices, which indeed correspond with the periodicities of $\Delta\delta^1H^N$ patterns (Figure S3). Thus, the helical curvature observed in the crystal structure of the isolated VSD is also present in DPC/LDAO micelles. The observed periodicity of $\Delta\delta^1H^N$ values is disrupted in the region connecting S4 and S45 helical elements (Figure 3). Moreover, the periodicity of the $\Delta\delta^1H^N$ pattern in S45 does not correspond with the curvature of this helical element in a crystal (Figure S3). These data additionally corroborate the proposal that in solution S4 and S45 behave as two independent helices, probably connected by a flexible hinge (see above).

In addition to the effects of the helical curvature, the observed $\Delta\delta^1H^N$ values may contain some other contributions created by the tertiary structure. The $\Delta\delta^1H^N$ shifts can be influenced by electrostatic interactions, including hydrogen bond formation and by effects of aromatic residues via so-called "ring-current" shifts.[35] The large (>1 ppm) $\Delta\delta^1H^N$ values observed for resonances of several residues in "regular" helices (S1, S2, and S3b) point to the proximity of corresponding amide groups and aromatic or charged moieties. Some of these shifts (Figure 3, filled diamonds) can be easily explained using the crystal structure of the isolated VSD. For example, the large downfield shift (+2.38 ppm) of $^1H^N$ Leu26 can be ascribed to the sum of ring-current and electrostatic effects arising from hydrogen bonding with the side chain of His24 and from the positive N-terminal charge of the S1 helical dipole (Figure S3). Downfield shifts of $^1H^N$ Trp70 and Ala74 (+1.44 and +1.02 ppm, respectively) can be attributed to "ring-current" shifts from neighboring Trp70 and Tyr75 residues (Figure S3).

The most prominent feature of the $\Delta\delta^1H^N$ pattern is a large downfield shift of $^1H^N$ Ala100 and Gly101 (+1.59 and +1.34 ppm, respectively), which cannot be ascribed by a contribution from the helical dipole of S3b. Inspection of the corresponding region from the crystal structure (Figure 4) explains observed shifts by involvement of Ala100 and Gly101 amide groups into the net of hydrogen bonds with the charged side chain of Asp62 in the S1 helix and an associated water molecule. Indeed, the presence of a tightly bound water molecule in the vicinity of Gly101 and the proximity of $^1H^N$ Gly101 and the aromatic ring of Tyr59 (S1) were confirmed by observation of the corresponding NOE cross-peaks on resonance frequencies of water and $^1H^\delta$ of Tyr59 (Figure 4). The large upfield shift (−1.45 ppm) observed for $^1H^N$ Val42 (S1) can be explained by disruption of the α-helical hydrogen bond pattern in the middle of helix S1 induced by the charged side chain of Arg133 (S4) (Figure 4). It is in agreement with the crystal structure of VSD, in which the salt bridge Asp62-Arg133 (S1−S4) is one of the major interhelical interactions that stabilize the packing of the VSD helical bundle.[21]

The measured ^1H, ^{13}C, and ^{15}N chemical shifts were compared with the available X-ray structures of VSD using the chemical shift calculation program SPARTA.[36] The comparison (see Supporting Information) indicated that the conformation of the domain in DPC/LDAO micelles is closest to that in the crystal of the isolated VSD. Only poor chemical shift correlations were observed with the structures of the full-length KvAP channel (Figure S4).

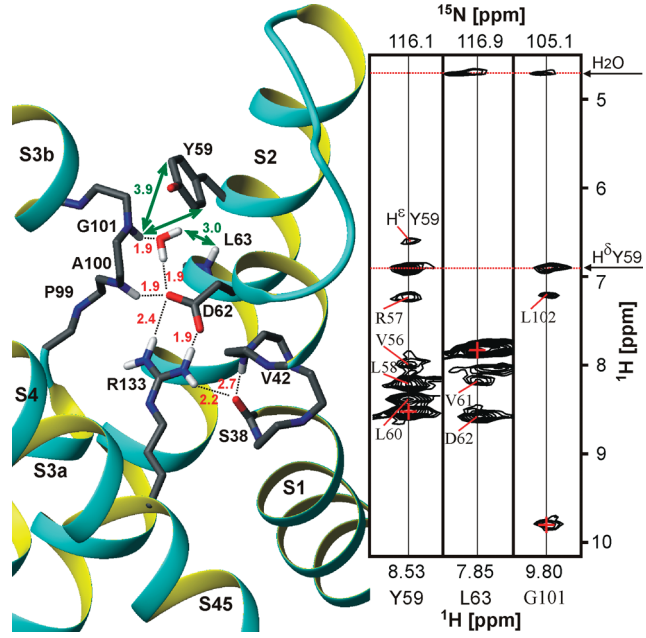

Figure 4. NMR data ($\Delta\delta^1H^N$ and NOE) obtained for micelle-solubilized the VSD are in agreement with the presence of an interhelical salt-bridge Asp62-Arg133 and associated tightly bound water molecule observed in the crystal structure of VSD (PDB 1ORS). The hydrogen bonding and proton−proton distances as measured in the crystal structure are shown in angstroms by red and green numbers, respectively. The involvement of $^1H^N$ of Ala100 and Gly101 in strong hydrogen bonds and disruption of the helical hydrogen bond at $^1H^N$ of Val42 are confirmed by $\Delta\delta^1H^N$. The presence of a tightly bound water molecule and spatial closeness of $^1H^N$ Gly101 with the aromatic ring of Tyr59 are confirmed by NOE contacts (green arrows). (Insert) The fragment of 150 ms ^{15}N-separated 3D HNH-NOESY spectrum measured using the $^2H,^{15}N$-labeled VSD (the estimated degree of ^2H incorporation in the protein is ∼85%). Diagonal cross-peaks are marked by red crosses; the ^1H resonance frequencies of water and $^1H^\delta$ Tyr59 are drawn by red dotted lines.

Backbone Dynamics of the Isolated VSD. The observation of a distribution in intensities of cross-peaks in the 3D HNCO spectrum (Figure 3) indicated the presence of significant intramolecular mobility within the VSD molecule. Strong or weak (relative to average) intensities of HNCO peaks are most probably the consequences of motions at ps−ns or μs−ms time scales, respectively. According to these data the extensive ps−ns motions are presented in N- and C-terminal regions, S1−S2 loop, and S23−S3a helices (Figure 6A). The most pronounced patches of μs−ms exchange fluctuations are located in the middle of S1 and S2 helices and in the hinges between S3a−S3b and S4−S45 helices (Figure 6B). Strong exchange broadening observed for HN of Leu26 at the chosen experimental conditions (pH 4.7) could be induced by proton exchange of the His24 side chain that is directly hydrogen bonded to the Leu26 amide group in the crystal structure. A slight increase of pH to 5.1 led to a detectable narrowing of the Leu26 signal (data not shown).

A more detailed investigation of backbone dynamics of the VSD solubilized in DPC/LDAO mixture was done using ^{15}N-relaxation measurements at 600 MHz. R_1 and R_2 relaxation rates and heteronuclear NOEs were measured using the $^2H,^{15}N$-labeled protein (Figure 5). Because of overlap in 2D $^1H,^{15}N$-correlation spectra and insufficient sensitivity in the case of exchange broadened signals, relaxation data were obtained for only 99 $^{15}N^H$ groups. The presence of extensive ps−ns motions in N- and C-terminal regions of the molecule (including the C-terminal half of S45) and in the S1−S2 loop was confirmed by low (<0.6) NOE values (Figures 5C, 6A). The extent of μs−ms fluctuations

(35) Asakura, T.; Taoka, K.; Demura, M.; Williamson, M. P. *J. Biomol. NMR* **1995**, *6*, 227–236.
(36) Shen, Y.; Bax, A. *J. Biomol. NMR* **2007**, *38*, 289–302.

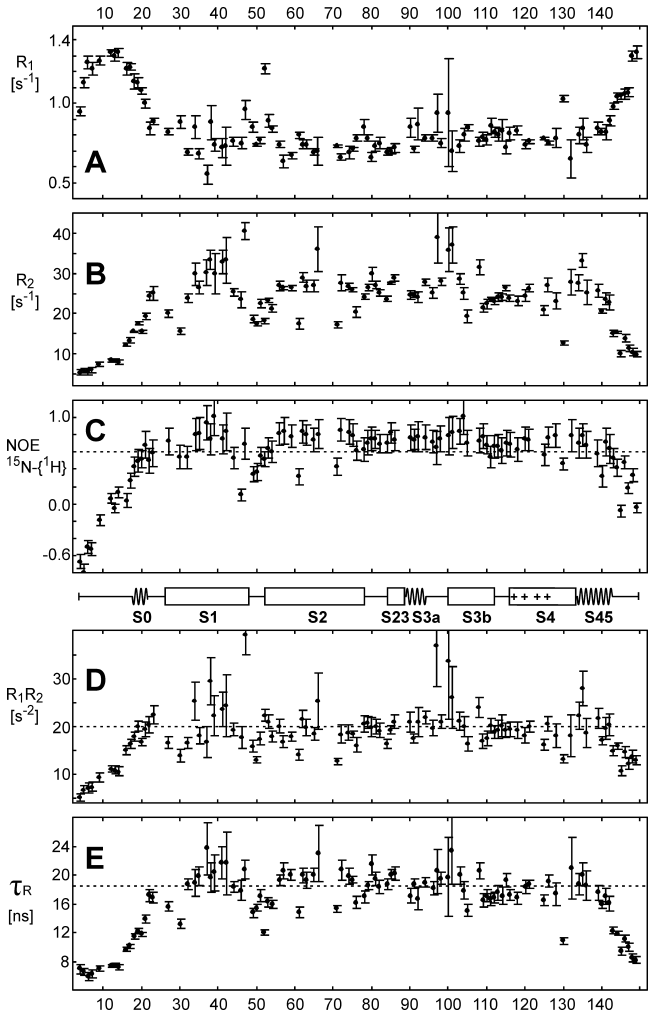

Figure 5. ^{15}N relaxation measurements reveal dynamical properties of the micelle-solubilized VSD. (A) R_1 rates, (B) R_2 rates, and (C) steady-state ^{15}N-{^{1}H}-NOE were measured at 600 MHz for a 1 mM sample of the ^{2}H,^{15}N-labeled VSD in a 100 mM perdeuterated d_{38}-DPC, 50 mM LDAO, pH 4.7, 45 °C. The residues displaying NOE < 0.6 are subjected to extensive motions on the ps−ns time scale. (D) Calculated $R_1 \cdot R_2$ product. The residues displaying $R_1 \cdot R_2 > 20$ s^{-2} are subjected to exchange fluctuations in the μs−ms time scale.[37] (E) The effective rotational correlation time was calculated from the R_2/R_1 ratio. The level corresponding to the average value (18.4 ns) calculated over "stable" regions (NOE > 0.6, $R_1 \cdot R_2 < 20$ s^{-2}) of the VSD is shown by a broken line. The secondary structure elements as determined by NMR are shown in the middle of the figure.

was deduced using the $R_1 \cdot R_2$ product as in ref 37. A large increase of $R_1 \cdot R_2$ values relative to the 20 s^{-2} level observed in the middle of the S1 and S2 helices and in the hinges between the S3a−S3b and S4−S45 helices (Figures 5D, 6B) indicates the presence of μs−ms exchange fluctuations in these regions of the VSD.

The effective rotational correlation time (τ_R) of the VSD/detergent complex was calculated from the R_2/R_1 ratio (Figure 5E). This graph also indicates the presence of some residues with nonaverage behavior that may be explained by μs−ms and ps−ns motions and/or rotation diffusion anisotropy of the VSD/detergent complex. The "average" τ_R value (18.4 ns) was calculated through the "stable" regions of the VSD displaying NOE > 0.6 and $R_1 \cdot R_2 < 20$ s^{-2}. This value corresponds to a

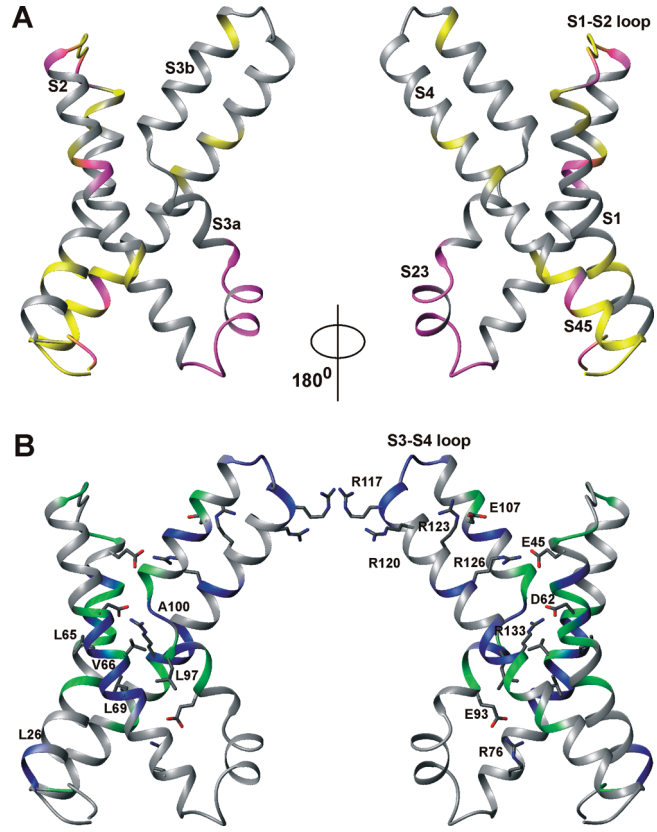

Figure 6. Dynamical NMR data mapped on the crystal structure of the VSD (PDB 1ORS). (A) The residues affected by dynamic processes on ps−ns the time scale. For residues in yellow, a heteronuclear NOE <0.6 was observed; successive pairs of residues ($i - 1$, i) shown in magenta correspond to signals for which an intensity of the HNCO cross-peaks was observed that was twice as large than the average. (B) The residues affected by dynamics on μs−ms time scale. Residues in green correspond to $R_1 \cdot R_2 > 21$ s^{-2} (this value was taken to minimize contribution of measurement errors); successive pairs of residues ($i - 1$, i) with an intensity of HNCO cross-peaks twice smaller than average are shown in blue. The conservative Arg residues, the salt-bridges that stabilize the VSD structure and the hydrophobic residues (Leu65, Val66, Leu69, Leu97) that form interhelical contacts and divide extracellular and intracellular faced water filled crevices are shown by sticks.

rotation of a globular particle with $R_H \approx 32$ Å and apparent MW ≈ 50 kDa. This is consistent with results of NMR translation diffusion measurements ($D_T \approx 0.90 \times 10^{-10}$ m^2/s, at 30 °C, $R_H \approx 31$ Å). The estimated radius fits indeed to the sum of the cross-sectional radius of the VSD (~10 Å)[21] and the length of the detergent molecule (~20 Å for DPC and LDAO). Thus, the VSD/detergent complex can be envisaged as a single protein molecule with a hydrophobic surface covered by a layer of detergent. This conclusion is also supported by the observation of NOE contacts between $^1H^N$ of the protein and the terminal methyl group of the detergent fatty chains (Figure S5).

Discussion

There are many indications that VSDs behave as structurally independent units. These domains loosely associate with PD in potassium voltage-gated channels[6,38] and can be grafted to voltage insensitive channels to confer voltage gating.[39] The

(37) Kneller, J. M.; Lu, M.; Bracken, C. *J. Am. Chem. Soc.* **2002**, *124*, 1852–1853.

(38) Vamvouka, M.; Cieslak, J.; Van, E. N.; Hubbell, W.; Gross, A. *Protein Sci.* **2008**, *17*, 506–517.

(39) Lu, Z.; Klem, A. M.; Ramu, Y. *Nature* **2001**, *413*, 809–813.

isolated VSD folds into the distinct spatial structure after heterologous expression in *E. coli*,[12,21] displays specific affinity against spider voltage-sensor toxins,[21] and remains monomeric in a lipid membrane or detergent micelles.[12] Moreover, recently two classes of membrane proteins, highly homologous to the VSD, were described: voltage-gated proton channels[40,41] and voltage-sensitive phosphatases that consist of a transmembrane VSD-like domain and a water-soluble enzymatic domain.[42] These data point to the validity of structural studies of isolated VSDs.

According to the results obtained by X-ray diffraction and EPR spectroscopy, the VSD of the KvAP channel in the activated state (at zero TM potential) represents a four-helical bundle, which has an overall hourglass shape with two water-filled crevices.[12,21,23] These crevices protrude from both sides of the lipid membrane to the central part of the domain, where specific helix−helix interactions and several salt bridges (e.g., Asp62-Arg133) fix the domain structure, stabilizing its spatial arrangement (see Figure 6).[21] In the present study, a good correspondence between NMR structural data and the structure of the VSD described above was found. First of all, the localization of the secondary structure elements and curvatures of transmembrane helices observed by NMR are very similar to those for the X-ray structure of the isolated VSD (Figures 3, S3). Second, the separation of S4−S45 structural elements into two independent helices (on the level of Ile131-Arg133) previously suggested by EPR was also observed in the present study. In addition, the detection by NMR of a tightly bound water molecule (near Asp62) and an enhanced solvent accessibility of the S23−S3a helical elements (Figures 3, S5) indirectly proves the presence of outer and inner water-filled crevices in the detergent solubilized VSD molecule. Finally, the secondary chemical shifts of the amide protons support the presence of the Asp62-Arg133 salt bridge in the environment of DPC/LDAO micelles (Figure 4). Based on these data, we conclude that the VSD in this medium adopts a conformation that corresponds to the activated state of the domain in open or open inactivated states of the KvAP channel.

The backbone of the VSD undergoes intramolecular motions at several time scales. Only few parts of the VSD are subjected to extensive dynamics on the ps−ns time scale (Figure 6A). These parts involve the N- and C-terminal regions of the domain (including C-terminal half of S45 helix), S1−S2 loop, and S23−S3a elements. In addition, the low amplitude of $\Delta\delta^{13}C^{\alpha}$ and $\Delta\delta^{13}C'$ and the absence of characteristic (i,i+3) NOE connectivities point to the enhanced mobility of the S45 helix (Figure 3). The observed flexibility of the S45 structural element is possibly associated with bending motions taking part in the hinge (Ile131-Arg133) connecting the S4 and S45 helices. Interestingly, the high-amplitude hinge-bending motions centered at Ile130, observed on the ns time scale, were recently also found by MD simulation of the isolated VSD.[43] The loop between the S3b and S4 helices, unlike other loops in the molecule, was found stable on the ps−ns time scale. This is in line with the observed protection from the solvent exchange and preservation of (i,i+2) and (i,i+3) NOE contacts in the region of the loop (Figure 3). We conclude that the S3b−S4 helical hairpin (so-called voltage-sensor paddle[21]) is rather rigid, as was also noted in the X-ray crystallography study.[21] In spite of the structural differences observed in other parts of the VSD, the S3b−S4 helical hairpin is very similar in all three crystal forms.[21,22]

The most intriguing feature of the intramolecular dynamics in the VSD is the presence of μs−ms exchange processes in the interior of the S1−S4 helical bundle (Figure 6B). This involves almost all residues from S1, S2, S3, and S4 helices that participate in interhelical contacts (around salt-bridge Asp62-Arg133) including Ala100, Gly101 (which contact with Asp62 through the network of electrostatic interactions, see Figure 4) and hydrophobic residues Leu65, Val66, Ala96, Leu97 that, according to MD simulations, divide extracellular and intracellular faced water filled crevices of the VSD.[43,44] The observation of a single set of NMR signals for all VSD residues indicates that the observed exchange process is fast on the chemical-shift time scale. Most probably, the fluctuations associated with this exchange process are of low amplitude in the region of the interhelical contacts and do not lead to a disruption of the Asp62-Arg133 salt bridge. It should be noted, however, that low-amplitude motions within this region may induce large-amplitude relative displacements of the helical termini and the loops, which may not be fully captured by the NMR relaxation measurements.

The μs−ms exchange fluctuations in the helical bundle of the VSD reflect the property of its helices to accomplish movements relative to each over. The extent of these dynamic processes in membrane mimicking media containing a lipid bilayer was evaluated by comparing the amplitudes of characteristic HN signals in 2D ^{1}H,^{15}N-TROSY spectra of the VSD measured in DPC micelles, DPC/LDAO micelles, and lipid−protein nanodiscs composed from DMPC, DMPG, and POPC/DOPG (3:1) lipids (Figure S8). Indeed, the exchange induced line broadening of the Ala100 and Gly101 amide groups was observed in all applied media, indicating the presence of the similar μs−ms interhelical fluctuations. Probably, these interhelical motions represent an inherent property of the VSD and may also take place in the full-length KvAP channel incorporated into the natural bilayer membrane.

The observed μs−ms interhelical motions demonstrate the fluidity of the system and suggest that the involved residues also play a role in large-scale VSD rearrangements that take place in the domain upon changes of the TM potential. Unfortunately, the amplitude and direction of these rearrangements cannot be deduced from the obtained dynamical data. Knowledge of the VSD structure at resting TM potentials, together with knowledge of its dynamics, is required for construction of a detailed model of voltage gating. For example, the S1−S2 loop, S23−S3a elements, and S45 helix are shown experimentally to be more flexible and may accommodate interhelical movement during voltage gating. The conformation of moieties of the VSD that are rigid on the ps−ns time scale (S1, S2 helices and S3b−S4 helical hairpin) are most probably conserved in this process.

Presently there are several putative models describing the conformational rearrangement of the VSD implicated in voltage gating.[3,4] The "helical-screw" model describes the transition from the resting state to the activated state by a movement of the helix S4 relative to other structural elements of the VSD.[10]

(40) Sasaki, M.; Takagi, M.; Okamura, Y. *Science* **2006**, *312*, 589–592.
(41) Ramsey, I. S.; Moran, M. M.; Chong, J. A.; Clapham, D. E. *Nature* **2006**, *440*, 1213–1216.
(42) Murata, Y.; Iwasaki, H.; Sasaki, M.; Inaba, K.; Okamura, Y. *Nature* **2005**, *435*, 1239–1243.
(43) Sands, Z. A.; Grottesi, A.; Sansom, M. S. *Biophys. J.* **2006**, *90*, 1598–1606.
(44) Sands, Z. A.; Sansom, M. S. *Structure* **2007**, *15*, 235–244.

This model implies a disruption of the helical hairpin S3b−S4 and contradicts the obtained dynamical data about the stability of this structural element on the ps−ns time scale. The observed pattern of intramolecular dynamics is more consistent with a modified "voltage-sensor paddle" model proposed for the mammalian Kv1.2/2.1 chimaeric channel.[6] In this model the transition from the resting to the activated state is caused by a displacement of the well-structured helical hairpin S3b−S4 relative to the S1 and S2 helices. The amplitude of this movement in the KvAP channel was observed in a recent study of the accessibility of avidin to different-length tethered biotin reagents.[45] These data indicate that the S3b−S4 structural element can move during voltage gating by more than 15 Å along the axis perpendicular to the plane of the lipid bilayer.[45] In line with this model, the recent combined fluorescence/NMR study of the isolated S3b−S4 helical hairpin from the KvAP channel indicated that the arginine-rich voltage-sensor paddle is located within the bilayered region in DMPC/DHPC bicelles and influences the dynamics of acyl chains and glycerol moieties of the lipids.[46]

The present investigation illustrates the progress that was achieved in solution NMR studies of integral α-helical membrane proteins during the past 10 years. The combination of relaxation optimized TROSY NMR experiments,[47] uniform deuteration,[48] and increased sensitivity provided by cryogenically cooled NMR probes allowed the routine structural analysis of one-TM and two-TM helices proteins.[13,49,50] In contrast, NMR studies of polytopic α-helical membrane proteins still remain challenging. There are only a few successful examples of such studies where backbone resonance assignment and structural characterization were achieved.[14,51−55] To the best of our knowledge, the current investigation of the VSD from the KvAP channel provides the first example of the polytopic α-helical membrane protein where the "slow" (μs−ms) interhelical dynamics were characterized in detail.

In summary, the structure and dynamics of the isolated voltage-sensing domain of the KvAP channel have been characterized by NMR. The obtained dynamical data in combination with published results of NMR studies of the KcsA channel (that represent the isolated pore domain)[51,52,56−59] provide a picture of diverse dynamical processes involved in the functioning of potassium channels and opens new perspectives for the understanding of molecular mechanisms involved in voltage gating.

Acknowledgment. This work was financially supported by the Russian Federal Agency for Science and Innovations, a Grant from the President of the Russian Federation, the Russian Academy of Science, and the Russian Foundation for Basic Research.

Supporting Information Available: Sample preparation, NMR spectra of VSD in different media, temperature coefficients of amide protons, residue-specific solvent and detergent accessibility of VSD, additional analysis of secondary chemical shifts. This material is available free of charge via the Internet at http://pubs.acs.org.

JA909752R

(45) Ruta, V.; Chen, J.; MacKinnon, R. *Cell* **2005**, *123*, 463–475.
(46) Biverstahl, H.; Lind, J.; Bodor, A.; Mäler, L. *Biochim. Biophys. Acta* **2009**, *1788*, 1976–1986.
(47) Pervushin, K.; Riek, R.; Wider, G.; Wuthrich, K. *Proc. Natl. Acad. Sci. U.S.A.* **1997**, *94*, 12366–12371.
(48) Tugarinov, V.; Kanelis, V.; Kay, L. E. *Nat. Protoc.* **2006**, *1*, 749–754.
(49) Bocharov, E. V.; Mayzel, M. L.; Volynsky, P. E.; Goncharuk, M. V.; Ermolyuk, Y. S.; Schulga, A. A.; Artemenko, E. O.; Efremov, R. G.; Arseniev, A. S. *J. Biol. Chem.* **2008**, *283*, 29385–29395.
(50) Sulistijo, E. S.; Mackenzie, K. R. *Biochemistry* **2009**, *48*, 5106–5120.
(51) Baker, K. A.; Tzitzilonis, C.; Kwiatkowski, W.; Choe, S.; Riek, R. *Nat. Struct. Mol. Biol.* **2007**, *14*, 1089–1095.
(52) Chill, J. H.; Louis, J. M.; Miller, C.; Bax, A. *Protein Sci.* **2006**, *15*, 684–698.
(53) Gautier, A.; Kirkpatrick, J. P.; Nietlispach, D. *Angew. Chem., Int. Ed.* **2008**, *47*, 7297–7300.
(54) Poget, S. F.; Cahill, S. M.; Girvin, M. E. *J. Am. Chem. Soc.* **2007**, *129*, 2432–2433.
(55) Van Horn, W. D.; Kim, H. J.; Ellis, C. D.; Hadziselimovic, A.; Sulistijo, E. S.; Karra, M. D.; Tian, C.; Sonnichsen, F. D.; Sanders, C. R. *Science* **2009**, *324*, 1726–1729.
(56) Chill, J. H.; Louis, J. M.; Baber, J. L.; Bax, A. *J. Biomol. NMR* **2006**, *36*, 123–136.
(57) Takeuchi, K.; Takahashi, H.; Kawano, S.; Shimada, I. *J. Biol. Chem.* **2007**, *282*, 15179–15186.
(58) Ader, C.; Pongs, O.; Becker, S.; Baldus, M. *Biochim. Biophys. Acta* **2010**, *1798*, 286–290.
(59) Ader, C.; Schneider, R.; Hornig, S.; Velisetty, P.; Wilson, E. M.; Lange, A.; Giller, K.; Ohmert, I.; Martin-Eauclaire, M. F.; Trauner, D.; Becker, S.; Pongs, O.; Baldus, M. *Nat. Struct. Mol. Biol.* **2008**, *15*, 605–612.